Inorganic Chemistry
Article

Inorg. Chem. **2010**, *49*, 5025–5032 **5025**
DOI: 10.1021/ic100106b

Highly Solvent Dependent Luminescence from $[Ru(bpy)_n(dppp2)_{3-n}]^{2+}$ ($n = 0-2$)

Yujie Sun and Claudia Turro*

Department of Chemistry, The Ohio State University, Columbus, Ohio 43210

Received January 18, 2010

The photophysical properties of a series of ruthenium(II) complexes possessing the dppp2 (dppp2 = pyrido-[2′,3′:5,6]pyrazino[2,3-*f*][1,10]phenanthroline) ligand, $[Ru(bpy)_n(dppp2)_{3-n}]^{2+}$ (bpy = 2,2′-bipyridine; $n = 0-3$), were investigated. The dppp2-containing complexes possess a remarkable solvent dependence of the luminescence maximum, lifetime, and quantum yield. For example, the emission maximum of $[Ru(bpy)_2(dppp2)]^{2+}$ blue shifts from 752 nm in CH_3CN to 653 nm in CH_2Cl_2, concomitant with a 19-fold enhancement in the luminescence quantum yield. Electronic structure calculations, transient absorption spectroscopy, and electrochemistry were also used to gain insight into the photophysical properties of the dppp2 complexes. The pronounced solvent effect of the emission of these complexes is attributed to the changes in the relative stabilities of two low-lying metal-to-ligand charge transfer (MLCT) excited states on the environment, where the lowest energy MLCT state is more sensitive to the polarity of the solvent than that which lies at slightly higher energy. Transient absorption spectroscopy shows that the identity of the lowest energy MLCT state does not change as a function of solvent, however, its emission maximum and lifetime are greatly affected by the polarity of the surrounding medium. In contrast to $[Ru(bpy)_2(dppz)]^{2+}$ (dppz = dipyrido[3,2-*a*:2′,3′-*c*]phenzine), the lowest energy excited state in the dppp2-containing complexes is assigned as arising from a triplet MLCT state where the charge is localized on the portion of the dppp2 ligand distal to the metal, $^3MLCT^{dis}$.

Introduction

Ruthenium polypyridyl complexes, such as $[Ru(bpy)_3]^{2+}$ (**1**, bpy = 2,2′-bipyridine, Figure 1a),[1] continue to be investigated extensively owing to their potential applications in solar energy conversion,[2,3] in sensing and signaling,[4−7] as therapeutic agents,[8−11] and in the storage of information.[4,12] Ru(II) complexes as luminescence-based sensors are particularly attractive because of their high sensitivity, ease of modification to obtain desired molecular structures, and the simplicity of use.[5,13−17]

In particular, Ru(II) complexes possessing ligands with extended π-systems, such as $[Ru(L)_2(dppz)]^{2+}$ (L = bpy or phen (1,10-phenanthroline); dppz = dipyrido[3,2-*a*:2′,3′-*c*]phenzine; ligand structures in Figure 1a), exhibit marked differences in luminescence quantum yields in water and organic solvents.[18,19] Ruthenium(II) complexes with dppz ligands are known to possess low-lying triplet metal-to-ligand charge transfer (^{3}MLCT) excited states localized on the π^* orbitals of the dppz ligand proximal ($^3MLCT^{prox}$, bpy) and distal ($^3MLCT^{dis}$, phenazine) to the metal (Figure 1b).[20,21] The lowest energy excited state in $[Ru(bpy)_2(dppz)]^{2+}$ has

*To whom correspondence should be addressed. E-mail: turro@chemistry.ohio-state.edu.

(1) Meyer, T. J. *J. Am. Chem. Soc.* **1989**, *22*, 163.
(2) Lewis, N. S.; Nocera, D. G. *Proc. Natl. Acad. Sci.* **2006**, *103*, 15729.
(3) Balzani, V.; Campagna, S.; Denti, G.; Juris, A.; Serroni, S.; Venturi, M. *Acc. Chem. Res.* **1998**, *31*, 26.
(4) de Silva, A. P.; Gunaratne, H. Q. N.; Gunnlaugsson, T.; Huxley, A. J. M.; McCoy, C. P.; Rademacher, J. T.; Rice, T. E. *Chem. Rev.* **1997**, *97*, 1515.
(5) Martinez-Manez, R.; Sancenon, F. *Chem. Rev.* **2003**, *103*, 4419.
(6) (a) Drummond, T. G.; Hill, M. G.; Barton, J. K. *Nat. Biotechnol.* **2003**, *21*, 1192. (b) Boon, E. M.; Ceres, D. M.; Drummond, T. G.; Hill, M. G.; Barton, J. K. *Nat. Biotechnol.* **2000**, *18*, 1096. (c) Hartshorn, R. M.; Barton, J. K. *J. Am. Chem. Soc.* **1992**, *114*, 5919.
(7) (a) Lutterman, D. A.; Chouai, A.; Sun, Y.; Stewart, C. D.; Dunbar, K. R.; Turro, C. *J. Am. Chem. Soc.* **2008**, *30*, 1163. (b) Sun, Y.; Lutterman, D. A.; Turro, C. *Inorg. Chem.* **2008**, *47*, 6427. (c) Liu, Y.; Chouai, A.; Degtyareva, N. N.; Dunbar, K. R.; Turro, C. *J. Am. Chem. Soc.* **2005**, *127*, 10796.
(8) (a) Liu, Y.; Turner, D. B.; Singh, T. N.; Chouai, A.; Dunbar, K. R.; Turro, C. *J. Am. Chem. Soc.* **2009**, *131*, 26. (b) Liu, Y.; Hammitt, R.; Lutterman, D. A.; Joyce, L. E.; Thummel, R. P.; Turro, C. *Inorg. Chem.* **2009**, *48*, 375. (c) Liu, Y.; Hammitt, R.; Lutterman, D. A.; Thummel, R. P.; Turro, C. *Inorg. Chem.* **2007**, *46*, 6011. (d) Singh, T. N.; Turro, C. *Inorg. Chem.* **2004**, *43*, 7260.
(9) Turro, N. J.; Barton, J. K. *J. Biol. Inorg. Chem.* **1998**, *3*, 201.
(10) Clarke, M. *Coord. Chem. Rev.* **2002**, *232*, 69.
(11) Erkkila, K. E.; Odom, D. T.; Barton, J. K. *Chem. Rev.* **1999**, *99*, 2777.
(12) de Silva, A. P. M.; McClenaghan, N. D. *Chem.—Eur. J.* **2004**, *10*, 574.
(13) (a) Callan, J. F.; Silva, A. P. d.; Magria, D. C. *Tetrahedron* **2005**, *61*, 8551. (b) Bryan, A. J.; de Silva, A. P.; De Silva, S. A.; Rupasinghe, R. A. D. D.; Sandanayake, K. R. A. S. *Biosensors* **1989**, *4*, 169.
(14) Fabbrizzi, L.; Licchelli, M.; Pallavicini, P. *Acc. Chem. Res.* **1999**, *32*, 846.
(15) (a) Baleizao, C.; Nagl, S.; Schaferling, M.; Berberan-Santos, M. N.; Wolfbeis, O. S. *Anal. Chem.* **2008**, *80*, 6449. (b) Nagl, S.; Wolfbeis, O. S. *Analyst* **2007**, *132*, 507.
(16) Sun, S.-S.; Lees, A. J. *Coord. Chem. Rev.* **2002**, *230*, 171.
(17) Molokanova, E.; Savchenko, A. *Drug Discovery Today* **2008**, *13*, 14.
(18) Nair, R. B.; Cullum, B. M.; Murphy, C. J. *Inorg. Chem.* **1997**, *36*, 962.
(19) Olson, E. J. C.; Hu, D.; Hormann, A.; Jonkman, A. M.; Arkin, M. R.; Stemp, E. D. A.; Barton, J. K.; Barbara, P. F. *J. Am. Chem. Soc.* **1997**, *119*, 11458.
(20) (a) Önfelt, B.; Lincoln, P.; Nordén, B. *J. Am. Chem. Soc.* **2001**, *123*, 3630. (b) Olofsson, J.; Önfelt, B.; Lincoln, P. *J. Phys. Chem. A* **2004**, *108*, 4391.

Published on Web 04/28/2010

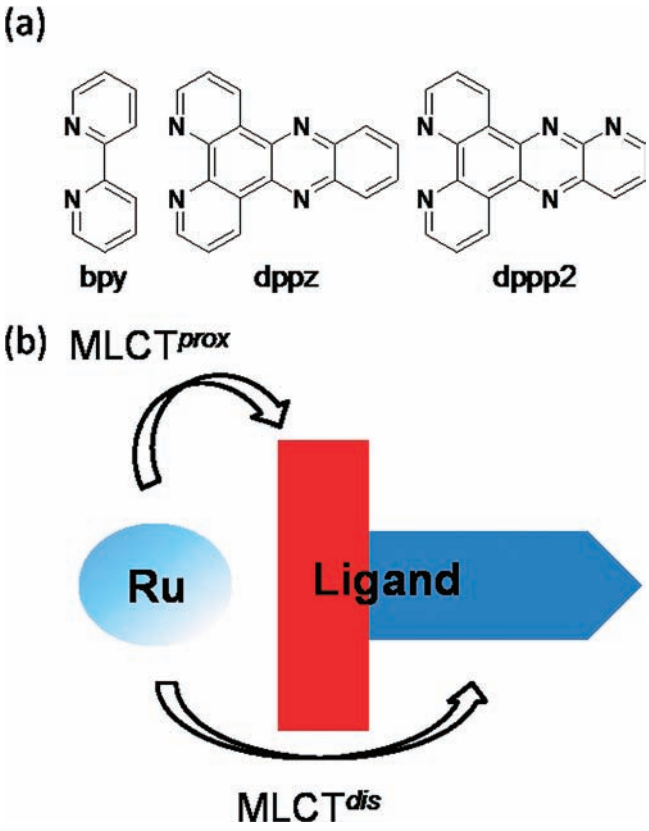

Figure 1. (a) Molecular structures of the ligands bpy, dppz, and dppp2 and (b) schematic representation of the MLCT transitions from the ruthenium center to a planar aromatic ligand with extended π-system showing $MLCT^{prox}$ and $MLCT^{dis}$.

been shown to be the nonemissive Ru→dppz $^3MLCT^{dis}$ state, whereas the luminescent $^3MCLT^{prox}$ lies at a higher energy.[20,21] The lack of luminescence from the $^3MLCT^{dis}$ state can be attributed to various factors, including the low energy of the excited state, resulting in increased nonradiative deactivation, and decreased electronic coupling due to the longer donor/acceptor distance compared to $^3MLCT^{prox}$.[20,21] The relative energy of the $^3MLCT^{prox}$ and $^3MLCT^{dis}$ states is dependent on the environment, resulting in marked population shifts as a function of solvent.[18,20,21] These changes in excited state energies have been used to explain the "DNA light-switch" effect, which takes place when the complex binds to DNA through intercalation of the dppz ligand.[22]

The solvent dependence of the luminescence of the dinuclear complex $[(L)_2Ru(tpphz)Ru(L)_2]^{4+}$ (L = bpy or phen) has also been reported, where tpphz (tetrapyrido[3,2-*a*:2′,3′-*c*:3″,2″-*h*:2‴,3″-*j*]phenazine) is a bridging ligand related to dppz.[7a,23] The emission maximum of $[(bpy)_2Ru(tpphz)Ru(bpy)_2]^{4+}$ shifts from 733 nm in CH_2Cl_2 to 749 nm in CH_3CN.[7a] Time-resolved absorption and luminescence lifetime measurements were used to investigate the excited state interconversion between the two low-lying ^3MLCT levels of $[(phen)_2Ru(tpphz)Ru(phen)_2]^{4+}$, where the decay of the $^3MLCT^{prox}$ state and the concomitant formation of $^3MLCT^{dis}$ occur in ~200 ps in CH_2Cl_2.[23] In contrast, the luminescence of $[Ru(bpy)_2(tpphz)]^{2+}$ depends weakly on solvent, with emission maxima of 613 and 627 nm in CH_2Cl_2 and CH_3CN, repectively.[7a]

The present work focuses on a series of mononuclear ruthenium polypyridyl complexes possessing the dppp2 (dppp2 = pyrido[2′,3′:5,6]pyrazino[2,3-*f*][1,10]phenanthroline) ligand, which is structurally related to dppz (Figure 1a). The photophysical properties of $[Ru(bpy)_2(dppp2)]^{2+}$ (**2**), $[Ru(bpy)(dppp2)_2]^{2+}$ (**3**), and $[Ru(dppp2)_3]^{2+}$ (**4**) were investigated and compared to those of **1** and related complexes. The luminescence maxima and lifetimes of **2**−**4** are highly dependent on solvent, and this effect is explained using electrochemical data and electronic structure calculations, among other techniques. This pronounced solvent dependence makes **2**−**4** potentially useful for sensing applications.

Experimental Section

Materials. 2,2′-Bipyridine (bpy), 1,10-phenanthroline (phen), 2,3-diaminopyridine, and ruthenium chloride hydrate were purchased from Aldrich and used as received. $Ru(bpy)_2Cl_2$,[24,25] 1,10-phenanthroline-5,6-dione (phendione),[26,27] and $[Ru(bpy)_3](PF_6)_2$ (**1**)[7b] were prepared according to literature methods. $Ru(dppp2)_2Cl_2$ was synthesized using the reported method for $Ru(bpy)_2Cl_2$, replacing bpy with dppp2.[24,25]

Dppp2. The dppp2 ligand was synthesized via the condensation of phendione and 2,3-diaminopyridine in a manner similar to that reported for tpphz.[28] ^1H NMR (400 MHz, *DMSO-d*$_6$) δ (ppm): 9.54 (dd, J = 8.10, 1.58 Hz, 1H), 9.49 (dd, J = 8.10, 1.56 Hz, 1H), 9.40 (dd, J = 3.94, 1.78 Hz, 1H), 9.24 (dt, J = 4.04, 4.03, 1.70 Hz, 2H), 8.82 (dd, J = 8.48, 1.71 Hz, 1H), 8.06 (dd, J = 8.46, 4.02 Hz, 1H), 7.96 (dt, J = 7.64, 7.61, 4.43 Hz, 2H). ESI-MS: m/z, 306.1, $[dppp2 + Na]^+$. Anal. Calcd for $C_{17}H_9N_5 \cdot 0.25H_2O$: C, 70.95; H, 3.33; N, 24.33. Found: C, 70.68; H, 3.30; N, 24.25.

$[Ru(bpy)_2(dppp2)](PF_6)_2$ (2). $Ru(bpy)_2Cl_2$ (22 mg) was refluxed under N_2 with 1 equiv of dppp2 (13 mg) in thoroughly deaerated 50/50 ethanol/water (10 mL) for 3 h. The mixture was allowed to cool to room temperature, and the complex was precipitated as a red solid by the addition of a saturated aqueous NH_4PF_6 solution. The precipitate was washed with water and diethyl ether and was dried under vacuum. The chloride salt of **2** was precipitated by the addition of Bu_4NCl to an acetone solution of **2**, as previously reported for related complexes,[7c] followed by column chromatography using Sephadex G-15 as the solid phase and eluted with 0.1 M NaCl. The orange eluate was dried under vacuum and was dissolved in $CHCl_3$ to separate the product from NaCl. The product was further purified via reverse-phase HPLC, eluted with a mixture of CH_3CN (38%) and 20 mM thiethanolamine acetate buffer (62%, pH = 7.5) at a flow rate of 5 mL/min, and precipitated with the addition of NH_4PF_6.[7a] Yield: 78%. ^1H NMR (400 MHz, *CD*$_3$*CN*) δ(ppm): 9.71 (dd, J = 8.24, 1.32 Hz, 1H), 9.63 (dd, J = 8.23, 1.31 Hz,

(21) (a) Brennaman, M. K.; Meyer, T. J.; Papanikolas, J. M. *J. Phys. Chem. A* **2004**, *108*, 9938. (b) Brennaman, M. K.; Alstrum-Acevedo, J. H.; Fleming, C. N.; Jang, P.; Meyer, T. J.; Papanikolas, J. M. *J. Am. Chem. Soc.* **2002**, *124*, 15094.
(22) Friedman, A. E.; Chambron, J. C.; Sauvage, J. P.; Turro, N. J.; Barton, J. K. *J. Am. Chem. Soc.* **1990**, *112*, 4960.
(23) (a) Campagna, S.; Serroni, S.; Bodige, S.; MacDonnell, F. M. *Inorg. Chem.* **1999**, *38*, 692. (b) Flamigni, L.; Encinas, S.; Barigelletti, F.; MacDonnell, F. M.; Kim, K.-J.; Puntoriero, F.; Campagna, S. *Chem. Commun.* **2000**, 1185. (c) Campagna, S.; Puntoriero, F.; Nastasi, F.; Bergamini, G.; Balzani, V. *Top. Curr. Chem.* **2007**, *280*, 117.
(24) Sullivan, B. P.; Salmon, D. J.; Meyer, T. J. *Inorg. Chem.* **1978**, *17*, 3334.
(25) Giordano, P. J.; Bock, C. R.; Wrighton, M. S. *J. Am. Chem. Soc.* **1978**, *100*, 6960.
(26) Zhang, Z. B.; Yan, W. P.; Fan, M. G. *Chin. J. Appl. Chem.* **2005**, *22*, 103.
(27) Bodige, S.; MacDonnell, F. M. *Tetrahedron Lett.* **1997**, *38*, 8159.
(28) Bolger, J.; Gourdon, A.; Ishow, E.; Launay, J. P. *Inorg. Chem.* **1996**, *35*, 2937.

1H), 9.47 (dd, J = 4.01, 1.92 Hz, 1H), 8.84 (dd, J = 8.57, 1.92 Hz, 1H), 8.53 (dd, J = 13.28, 8.11 Hz, 4H), 8.19 (ddd, J = 5.37, 2.58, 1.33 Hz, 2H), 8.11 (dt, J = 7.99, 7.96, 1.65 Hz, 2H), 8.08 (dd, J = 8.52, 3.97 Hz, 1H), 8.01 (dt, J = 8.05, 7.99, 1.46 Hz, 2H), 7.90 (dd, J = 8.24, 5.39 Hz, 2H), 7.84 (ddd, J = 5.65, 1.39, 0.63 Hz, 2H), 7.73 (t, J = 4.37, 4.37 Hz, 2H), 7.46 (t, J = 6.64, 6.64 Hz, 2H), 7.25 (tdd, J = 7.07, 5.69, 1.33, 1.33 Hz, 2H). MALDI MS: m/z, $[Ru(bpy)_2(dppp2)]^+$, 697.3. Anal. Calcd for $C_{37}H_{25}F_{12}N_9P_2Ru \cdot 2H_2O$: C, 43.45; H, 2.86; N, 12.33. Found: C, 43.28; H, 2.49; N, 11.91.

[Ru(bpy)(dppp2)$_2$](PF$_6$)$_2$ (3). $[Ru(bpy)(dppp2)_2](PF_6)_2$ was prepared by the coordination of 1 equiv of bpy to $Ru(dppp2)_2Cl_2$ and purified by the method described for **2**. Yield: 83%. ^{1}H NMR (400 MHz, *acetone-d_6*) δ (ppm): 9.83 (dd, J = 8.26, 1.26 Hz, 2H), 9.73 (dd, J = 8.16, 1.21 Hz, 2H), 9.60 (d, J = 8.18 Hz, 2H), 8.96 (dd, J = 11.72, 8.73 Hz, 2H), 8.91 (d, J = 7.95 Hz, 2H), 8.73 (t, J = 4.60, 4.60 Hz, 2H), 8.64 (dd, J = 8.86, 4.20 Hz, 2H), 8.33−8.22 (m, 4H), 8.24−8.18 (m, 4H), 8.06−7.92 (m, 2H), 7.51 (m, 2H). MALDI MS: m/z, 970.7, $[Ru(bpy)(dppp2)_2](PF_6)^+$. Anal. Calcd for $C_{44}H_{26}F_{12}N_{12}P_2Ru \cdot 4H_2O$: C, 44.57; H, 2.89; N, 14.17. Found: C, 44.66; H, 2.93; N, 13.77.

[Ru(dppp2)$_3$](PF$_6$)$_2$ (4). $RuCl_3 \cdot 2H_2O$ (0.10 g) was refluxed with 10-fold excess dppp2 in ethylene glycol under N_2 for 8 h.[29] The mixture was allowed to cool to room temperature, and the complex was precipitated as a dark red solid by the addition of a saturated aqueous NH_4PF_6 solution. The precipitate was washed with water and diethyl ether and dried under vacuum. Yield: 89%. ^{1}H NMR (400 MHz, *CD_3CN*) δ (ppm): 9.75 (d, J = 8.10 Hz, 3H), 9.68 (dd, J = 8.26, 1.03 Hz, 3H), 9.49 (dd, J = 4.03, 1.87 Hz, 3H), 8.86 (dd, J = 8.58, 1.88 Hz, 3H), 8.37 (dd, J = 5.19, 3.41 Hz, 6H), 8.10 (dd, J = 8.59, 4.03 Hz, 3H), 7.88 (dd, J = 8.23, 5.47 Hz, 6H). MALDI MS: m/z, 1096.1, $[Ru(dppp2)_3](PF_6)^+$. Anal. Calcd for $C_{51}H_{27}F_{12}N_{15}P_2Ru \cdot 0.5H_2O$: C, 49.01; H, 2.26; N, 16.81. Found: C, 49.08; H, 2.53; N, 16.65.

Instrumentation. ^{1}H NMR spectra were obtained on a 400 MHz Bruker system. Electronic absorption spectra were collected on a Hewlett-Packard diode array spectrometer (HP 8453) equipped with HP 8453 WinSystem software. Emission spectra were recorded on a SPEX Fluoromax-2 spectrometer and transient absorption spectra were recorded on an instrument described previously.[7,8] Emission lifetime measurements were conducted at room temperature using an Edinburgh Instruments (FL920) single-photon-counting instrument, and the lifetimes were fitted using the Edinburgh Instruments nF900 software. Cyclic voltammograms were obtained on a Cypress Systems CS-1200 instrument in a single-compartment three-electrode cell. A Hewlett-Packard HP 1100 series HPLC was used in the purification. Elemental analysis was performed by Galbraith Laboratories (Knoxville, TN), MALDI-TOF mass spectrometry was performed on a Bruker Reflex III mass spectrometer with 2,5-dihydroxybenzoic acid as the matrix, and ESI mass spectrometry was conducted on a Bruker Micro-TOF instrument.

Methods. Deoxygenation for the luminescence experiments was performed by bubbling each sample with argon for 15 min and keeping it under positive argon pressure during the experiment. Emission quantum yields were calculated using $[Ru(bpy)_3]^{2+}$ in deoxygenated CH_3CN (Φ_{em} = 0.062) as the reference actinometer with λ_{exc} = 440 nm.[30,31] The radiative and nonradiative decay rates, k_r and k_{nr}, respectively, were calculated from $k_r = \Phi_{em}/\tau$ and $k_{nr} = 1/\tau - k_r$, where τ represents the emission lifetime. Cyclic voltammograms were measured in distilled acetonitrile containing 0.1 M Bu_4NPF_6 as the supporting electrolyte, using a glassy carbon working electrode, a platinum auxiliary electrode, and a Ag/AgCl reference electrode. At the end of each experiment, a small amount of ferrocene (Fc) was added as an internal standard, and $E_{1/2}(Fc^{+/0}) = +0.66$ V vs NHE was used as the reference for calculating the oxidation and reduction potentials of samples.[28]

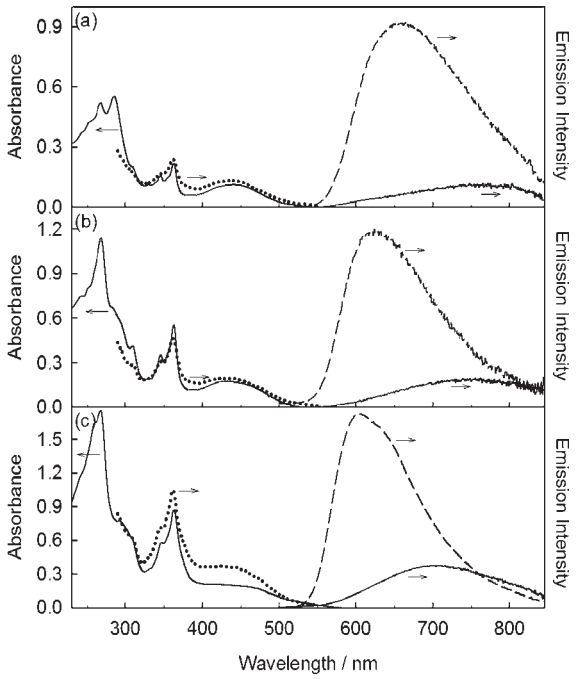

Figure 2. Electronic absorption (—), emission (—, λ_{exc} = 440 nm), and excitation spectra (· · · ·) spectra in CH_3CN of (a) 15 μM **2** (λ_{em} = 752 nm), (b) 7 μM **3** (λ_{em} = 740 nm), and (c) 6 μM **4** (λ_{em} = 705 nm), along with emission spectra (− − −, λ_{exc} = 440 nm) in CH_2Cl_2 at 298 K.

All calculations were performed with the *Gaussian 03* program package employing the DFT method with Becke's three-parameter hybrid functional and Lee−Yang−Parr's gradient-corrected correlation functional (B3LYP).[32,33] The Stuttgart/Dresden (SDD) basis set and effective core potential were used for the Ru atom,[34] and the 6-31G* basis set was applied for H, C, and N.[35] The geometries of the ground state and

(29) Bodige, S.; Torres, A. S.; Maloney, D. J.; Tate, D.; Kinsel, G. R.; Walker, A. K.; MacDonnell, F. M. *J. Am. Chem. Soc.* **1997**, *119*, 10364.
(30) Calvert, J. M.; Caspar, J. V.; Binstead, R. A.; Westmoreland, T. D.; Meyer, T. J. *J. Am. Chem. Soc.* **1982**, *104*, 6620.
(31) Crosby, G. A.; Demas, J. N. *J. Phys. Chem.* **1971**, *75*, 991.
(32) Frisch, M. J.; Trucks, G. W.; Schlegel, H. B.; Scuseria, G. E.; Robb, M. A.; Cheeseman, J. R.; Montgomery, J. A., Jr.; Vreven, T.; Kudin, K. N.; Burant, J. C.; Millam, J. M.; Iyengar, S. S.; Tomasi, J.; Barone, V.; Mennucci, B.; Cossi, M.; Scalmani, G.; Rega, N.; Petersson, G. A.; Nakatsuji, H.; Hada, M.; Ehara, M.; Toyota, K.; Fukuda, R.; Hasegawa, J.; Ishida, M.; Nakajima, T.; Honda, Y.; Kitao, O.; Nakai, H.; Klene, M.; Li, X.; Knox, J. E.; Hratchian, H. P.; Cross, J. B.; Bakken, V.; Adamo, C.; Jaramillo, J.; Gomperts, R.; Stratmann, R. E.; Yazyev, O.; Austin, A. J.; Cammi, R.; Pomelli, C.; Ochterski, J. W.; Ayala, P. Y.; Morokuma, K.; Voth, G. A.; Salvador, P.; Dannenberg, J. J.; Zakrzewski, V. G.; Dapprich, S.; Daniels, A. D.; Strain, M. C.; Farkas, O.; Malick, D. K.; Rabuck, A. D.; Raghavachari, K.; Foresman, J. B.; Ortiz, J. V.; Cui, Q.; Baboul, A. G.; Clifford, S.; Cioslowski, J.; Stefanov, B. B.; Liu, G.; Liashenko, A.; Piskorz, P.; Komaromi, I.; Martin, R. L.; Fox, D. J.; Keith, T.; Al-Laham, M. A.; Peng, C. Y.; Nanayakkara, A.; Challacombe, M.; Gill, P. M. W.; Johnson, B.; Chen, W.; Wong, M. W.; Gonzalez, C.; Pople, J. A. *Gaussian 03, revision C.02*; Gaussian, Inc.: Wallingford, CT, 2004.
(33) (a) Becke, A. D. *Phys. Rev. A: Gen. Phys.* **1988**, *38*, 3098. (b) Becke, A. D. *J. Chem. Phys.* **1993**, *98*, 5648. (c) Lee, C.; Yang, W.; Parr, R. G. *Phys. Rev. B: Condens. Matter Phys.* **1988**, *37*, 785.
(34) (a) Dolg, M.; Stoll, H.; Preuss, H. *Theor. Chim. Acta* **1993**, *85*, 441. (b) Wedig, U.; Dolg, M.; Stoll, H. *Quantum Chemistry: The Challenge of Transition Metals and Coordination Chemistry*; Kluwer Academic Publishers: Dordrecht, The Netherlands, 1986.
(35) Hehre, W. J.; Radom, L.; Schleyer, P. v. R.; Pople, J. A. *Ab Initio Molecular Orbital Theory*; John Wiley & Sons: New York, 1986.

Table 1. Absorption Maxima, Emission Maxima, Quantum Yields, and Electrochemistry of **1**−**4** in CH_3CN at 298 K

Complex	λ_{abs}/nm (ε/ × 10^3 M^{-1} cm^{-1})	λ_{em}/nm	Φ_{em}[a]	$E_{1/2}$[b]/V 3+/2+	2+/+	+/0
1	287 (75.5), 450 (13.0)	619	0.062	+1.54	−1.07	−1.26
2	268 (52.1), 286 (55.2), 345 (15.9), 362 (21.9), 440 (11.7)	752	0.002	+1.60	−0.50	−1.16
3	269 (113.7), 345 (35.2), 362 (55.1), 440 (17.3)	740	0.003	+1.61	−0.53	−1.02[c]
4	268 (161.1), 345 (48.5), 363 (79.5), 440 (20.1)	705	0.008	+1.59	−0.59	−0.84

[a] Error: ±0.001. [b] 0.1 M Bu_4NPF_6; vs NHE. [c] Quasi-reversible.

Table 2. Emission Maxima, Lifetimes, and Calculated Rate Constants of Radiative and Nonradiative Decay of **1**−**4** in CH_3CN/CH_2Cl_2 Mixtures at 298 K

	λ_{em}/nm (τ/ns)[b]				k_{nr}/ × 10^6 s^{-1}[b]				k_r/ × 10^4 s^{-1}[b]			
$F_{CH_2Cl_2}$[a]	**1**	**2**	**3**	**4**	**1**	**2**	**3**	**4**	**1**	**2**	**3**	**4**
0.0	619 (890)	752 (35)	740 (68)	705 (152)	1.1	28	15	6.5	7.0	5.7	4.4	5.3
0.2	615 (820)	750 (57)	720 (129)	695 (205)	1.1	18	7.7	4.8	7.8	5.3	4.7	8.8
0.4	611 (802)	735 (80)	700 (200)	679 (294)	1.2	12	5.0	3.3	7.9	6.3	5.0	10
0.6	608 (745)	705 (128)	670 (280)	656 (404)	1.3	7.7	3.5	2.4	8.7	7.8	5.7	12
0.8	602 (665)	680 (178)	644 (400)	627 (471)	1.4	5.5	2.4	2.0	8.5	12	6.3	15
1.0	600 (604)	653 (273)	625 (440)	604 (314)	1.6	3.5	2.2	3.0	8.6	14	7.3	19

[a] Volume fraction of CH_2Cl_2 in CH_3CN given by $F_{CH_2Cl_2} = V_{CH_2Cl_2}/(V_{CH_2Cl_2} + V_{CH_3CN})$. [b] Error: ±15%.

the lowest triplet state of **1**−**4** were optimized in acetonitrile and dichloromethane using the conductive polarizable continuum model method (CPCM). The local minimum on each potential energy surface was confirmed by frequency analysis. The dipole moment of each complex was calculated using the corresponding optimized geometries of the ground state and the lowest triplet state. The electronic orbitals were visualized using Chem3D Ultra 9.0.

Results and Discussion

Photophysical Properties and Electrochemistry in CH_3CN. The electronic absorption, excitation, and emission (λ_{exc} = 440 nm) spectra of **2**−**4** in deaerated CH_3CN at 298 K are shown in Figure 2, and the latter are compared to the corresponding emission spectra in CH_2Cl_2. As listed in Table 1, **2** exhibits a ligand-centered (LC) $\pi\pi^*$ transition localized on bpy with a maximum at 286 nm in CH_3CN, similar to that at 287 nm in **1**.[36] A peak at 268 nm is observed in **2**, which appears at 269 and 268 nm in **3** and **4**, respectively, and is attributed to a LC transition of dppp2. In addition, two transitions also associated with the dppp2 ligand are observed at ∼345 and ∼262 nm in **2**−**4** (Figure 2 and Table 1). Complexes **2**−**4** exhibit broad metal-to-ligand charge transfer (MLCT) transitions with maxima at 440 nm (Table 1), similar to that observed for **1**, with a maximum at 450 nm.[36]

Table 1 also lists the electrochemical data collected for **1**−**4** in CH_3CN, which exhibit one reversible Ru-based oxidation and several ligand-based reduction waves, as is typical of Ru(II) complexes.[36] As expected, the oxidation potentials, $E_{1/2}([Ru]^{3+/2+})$, are similar in **1**−**4**, consistent with other ruthenium polypyridyl complexes that possess metal-based highest occupied molecular orbitals (HOMOs) with little contribution from the ligands.[36,37] In contrast, the dppp2-localized first reduction potentials, $E_{1/2}([Ru]^{2+/+})$, vary significantly among the complexes in the series. The bpy-localized reduction of **1** at −1.07 V vs NHE is consistent with previously reported values.[36,38] The $E_{1/2}([Ru]^{2+/+})$ values of **2**−**4** are shifted to more positive potentials, −0.50, −0.53, and −0.59 V vs NHE, respectively, as expected for ruthenium complexes possessing ligands with extended π-systems that are easier to reduce than bpy.[36] It should be noted that the homoleptic complex **4** is slightly harder to reduce than **2** and **3** by 0.09 and 0.06 V, respectively, indicating that the lowest unoccupied molecular orbital (LUMO) in the former lies at slightly higher energy than those in the latter. Therefore, the invariance of the MLCT absorption maxima of **1**−**4** indicates that this electronic transition in **2**−**4** is not associated with the corresponding LUMO. This point is discussed in greater detail in the sections to follow.

The emission maxima (λ_{em}) and quantum yieds (Φ_{em}) of **1**−**4** in CH_3CN at 298 K are listed in Table 1. The emission maxima of **2**−**4** in CH_3CN are at significantly lower energy than that of **1**, consistent with an MLCT excited state where the charge transferred is localized on the dppp2 ligand and not on the ancillary bpy ligands. The excitation spectra of **2**−**4** monitored at the emission maximum of each complex at room temperature overlap well with the corresponding absorption spectra in both CH_3CN and CH_2Cl_2 (Figure 2), indicating that the luminescence of the dppp2 complexes does not originate from a highly emissive impurity. The maxima of the luminescence spectra of **2**−**4** at 77 K in EtOH/MeOH (v/v = 4:1) blue shift to 650, 610, and 600 nm, respectively, as is typical of Ru(II) complexes.[36] Unlike the 77 K emission spectrum of **1** under similar experimental conditions, those collected for **2**−**4** are broad with no clear vibronic structure.

It is evident from Table 1 that in CH_3CN the emission maximum blue shifts from 752 nm in **2** to 740 and 705 nm in **3** and **4**, respectively, with a concomitant increase in quantum yield. The longer lifetime and Φ_{em} of **1** compared to those of **2**−**4** in CH_3CN (Tables 1 and 2) can be attributed to the higher energy of the emission maximum

(36) Juris, A.; Balzani, V.; Barigelletti, F.; Campagna, S.; Belser, P.; Von Zelewsky, A. *Coord. Chem. Rev.* **1988**, *84*, 85.
(37) Fees, J.; Kaim, W.; Moscherosch, M.; Matheis, W.; Klima, J.; Krejcik, M.; Zalis, S. *Inorg. Chem.* **1993**, *32*, 166.
(38) Elliott, C. M.; Hershenhart, E. J. *J. Am. Chem. Soc.* **1982**, *104*, 7519.

of the former, as expected from the energy gap law.[36] The trend of the dppp2-localized reduction potentials, $E_{1/2}([Ru]^{2+/+})$, of these complexes in CH_3CN is also consistent with the blue shift of the emission maxima from **2** to **4** in the same solvent (Table 1). For comparison, the first reduction potential of $[Ru(bpy)_2(dppz)]^{2+}$ was reported to be −0.73 V vs NHE, which lies at a more negative potential than those of **2**−**4**, but with a similar oxidation potential (+1.57 V vs NHE).[36] Accordingly, the emission maximum of $[Ru(bpy)_2(dppz)]^{2+}$ in CH_3CN has a maximum at higher energy (~630 nm) than those of **2**−**4** (Table 1).[7b]

The strong luminescence of the homoleptic complex **1** arises from its charge transfer excited state where the charge is localized on the bpy ligands, which are similar to $^3MLCT^{prox}$ depicted in Figure 1b for the dppp2 complexes **2**−**4**. The lower energy emission maxima of **2**−**4** stem from ^3MLCT transitions where the transferred electron is localized on the dppp2 ligand. The shorter lifetimes and lower quantum yields of the luminescence of **2**−**4** compared to that of **1** can be explained by the presence of low-lying dppp2-based $^3MLCT^{dis}$ states in the former, which lie at lower energy than $^3MLCT^{prox}$.

The radiative and nonradiative decay rate constants, k_r and k_{nr}, respectively, were also determined for **1**−**4** (Table 2). The values of k_r and k_{nr} of **1** in CH_3CN are similar to those reported for $[Ru(dmb)_3]^{2+}$ (dmb = 4,4′-dimethyl-2,2′-bipyridine) in the same solvent, 8.3×10^4 and 1.06×10^6 s^{-1}, respectively,[39] although the dd excited states were not considered in the calculation of k_r and k_{nr}. Similarly, $k_r = 7.7 \times 10^4$ s^{-1} and $k_{nr} = 4.8 \times 10^5$ s^{-1} were previously reported for **1** in CH_3CN.[40] The lower energy excited states in **2**−**4** are expected to nonradiatively decay more efficiently to the ground state compared to that of **1** at higher energy, thus resulting in shorter luminescent lifetimes and lower quantum yields in the former.[20,21] The values of k_{nr} measured for **2**−**4** are consistent with the energy-gap law and are significantly greater than that of **1** in CH_3CN, whereas the values of k_r of the four complexes are of similar magnitude (Table 2). For **2** in CH_3CN, the calculated values of k_r and k_{nr} are comparable to those of $[(bpy)_2Ru(tpphz)Ru(bpy)_2]^{4+}$ ($k_r = 7.0 \times 10^4$ s^{-1} and $k_{nr} = 1.1 \times 10^7$ s^{-1}) with emission maximum at 749 nm in CH_3CN.[7a,23] In general, greater k_{nr} values contribute to the lower emission quantum yields and shorter lifetimes of **2**−**4** in CH_3CN compared to those of **1**. The solvent dependence of these values is discussed in the following section.

Solvent Dependence. The solvent dependence of the photophysical properties of $[Ru(phen)_2(dppz)]^{2+}$ has been previously investigated.[18] In nonqueous solvents, the luminescence lifetime and quantum yield of the complex show a clear relationship with the polarity of the medium. Changes in these quantities do not fit well with the hydrogen-bonding ability of the solvent, a factor that was proposed in early work to affect its spectroscopic properties.[22] The emission maximum of $[Ru(phen)_2(dppz)]^{2+}$ does not vary significantly within a series of nonaqueous solvents with a wide range of polarities, shifting only 34 nm (917 cm^{-1}) from CH_2Cl_2 to DMSO, with maxima that include 592 nm in CH_2Cl_2, 607 nm in CH_3CN, and 626 nm in DMSO.[18] In contrast, complexes **2**−**4** exhibit a substantially greater shift in emission maxima from CH_2Cl_2 to CH_3CN, and in CH_3CN/CH_2Cl_2 mixtures, together with significant changes in the luminescence lifetime and quantum yield.

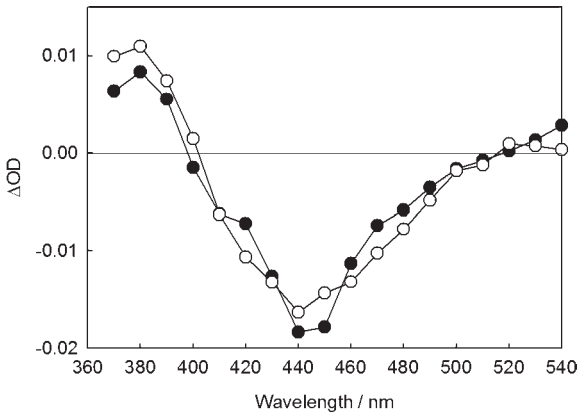

Figure 3. Transient absorption spectra of **2** in CH_3CN (●, 75 μM) and CH_2Cl_2 (○, 26 μM) collected at 24 and 160 ns after the laser pulse, respectively.

The absorption spectra of **2**−**4** are nearly identical in CH_2Cl_2 and CH_3CN, as previously reported for **1**.[40] In contrast, the emission spectra of **2**−**4** vary noticeably with increasing volume fraction of CH_2Cl_2 in CH_3CN. The emission maximum of **2** shifts from 752 nm in CH_3CN to 653 nm in CH_2Cl_2 (2016 cm^{-1}), and those of **3** and **4** blue shift 115 nm (2487 cm^{-1}) and 101 nm (2372 cm^{-1}), respectively, in the same solvents (Table 2). Additionally, only weak luminescence ($\Phi_{em} = 0.002$) with a short lifetime (35 ns) was measured for **2** in CH_3CN, with a 19-fold greater intensity ($\Phi_{em} = 0.038$) and an 8-fold increase in lifetime (273 ns) in CH_2Cl_2 (Table 2).

The emission maximum of **2**−**4** shifts uniformly with solvent composition in CH_2Cl_2/CH_3CN mixtures, without a distinct break in the trend. The emission lifetime of each complex increases with CH_2Cl_2 fraction, and each decay can be fitted to a monoexponential function at each solvent composition. These results are indicative of a gradual energy shift of the lowest energy state, $^3MLCT^{dis}$, in **2**−**4** as the polarity of the surrounding medium is tuned. Interactions with $^3MLCT^{prox}$ at higher energy may also play a role in the observed solvent dependence. It would be expected, however, that changes in the polarity of the surrounding medium would have a greater effect on the energy of $^3MLCT^{dis}$ than $^3MLCT^{prox}$, as discussed in more detail below.

The transient absorption spectra of **2** in deoxygenated CH_3CN and CH_2Cl_2 are shown in Figure 3 (λ_{exc} = 355 nm, fwhm ~8 ns). It is apparent from Figure 3 that the spectral profiles in the two solvents are superimposable, dominated by the bleach of the ground state absorption and positive signal with a maximum at ~380 nm, consistent with the same ^3MCLT excited state in CH_3CN and CH_2Cl_2. The transient absorption signal at 440 nm in CH_2Cl_2 was fitted to a monoexponential decay resulting in τ = 298 ns, and although in CH_3CN the signal was within the temporal resolution

(39) Damrauer, N. H.; Boussie, T. R.; Devenney, M.; McCusker, J. K. *J. Am. Chem. Soc.* **1997**, *119*, 8253.
(40) Caspar, J. V.; Meyer, T. J. *J. Am. Chem. Soc.* **1983**, *105*, 5583.

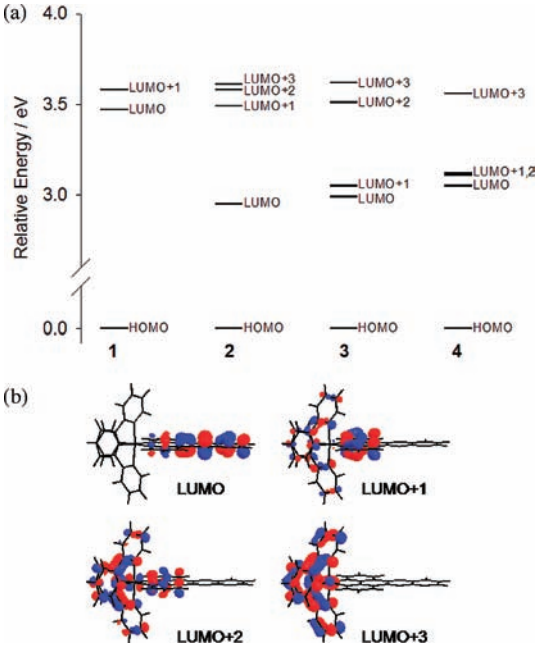

Figure 4. (a) Calculated molecular orbital diagrams of **1**−**4** and (b) electron density of selected unoccupied molecular orbitals of **2** (isovalue = 0.04).

of the instrument, the lifetime at 440 nm can be estimated to be ~40 ns. In 50:50 CH_3CN/CH_2Cl_2 (v/v) the lifetime of the transient signal at 440 nm was ~100 ns, also in agreement with the emission data (Table 2). The similarity of the transient absorption and emission lifetimes (Table 2) indicates that both signals arise from the same excited state of **2** in each solvent and in the mixture, $^3MLCT^{dis}$.

The values of k_r and k_{nr} were also determined for each complex as a function of CH_2Cl_2 volume fraction in CH_3CN and are listed in Table 2. Consistent with previous results, little variation is observed for the k_r and k_{nr} values of **1** with increasing CH_2Cl_2.[40] In contrast, the radiative decay rate constants, k_r, of **2**−**4** decrease with increasing solvent polarity (decreasing the volume fraction of CH_2Cl_2 in CH_3CN). It is also evident from Table 2 that the value of k_{nr} of **2**−**4** is sensitive to the medium, with an 8-fold increase measured for **2** from CH_2Cl_2 to CH_3CN. Similarly, the values of k_{nr} of **3** and **4** increase by factors of 7 and 2, respectively, in the same solvents. In contrast, the magnitude of both k_r and k_{nr} of the emission of the $^3MLCT^{prox}$ of $[Ru(phen)_2(dppz)]^{2+}$ have been reported to be relatively unaffected as the solvent is varied from CH_3CN to CH_2Cl_2.[18] In general, the k_{nr} values of **2**−**4** are greater than those of other typical ruthenium polypyridyl complexes in CH_3CN, while the k_r values are similar to others.[7,36,39]

Electronic Structure Calculations. Density functional theory calculations were performed to aid in the understanding of the photophysical properties of **1**−**4**. The calculated molecular orbital (MO) diagrams of **1**−**4** are compared in Figure 4a. Since the metal-centered oxidation potentials of **1**−**4** are similar (Table 1), the HOMOs of the four complexes were set at 0.0 eV in Figure 4a. The LUMOs of **2**, **3**, and **4** were calculated to lie 0.52, 0.48, and 0.42 eV below the LUMO of **1**, which correspond well to the measured difference in $E_{1/2}([Ru]^{2+/+})$ values of **2**−**4**

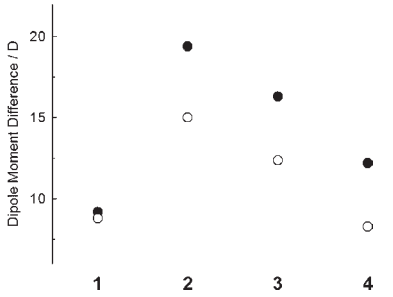

Figure 5. Calculated dipole moment difference between the ground state and the lowest energy triplet state of **1**−**4** in CH_3CN (●) and CH_2Cl_2 (○).

compared to that of **1** (Table 1). The LUMOs of the heteroleptic complexes **2** and **3** were calculated to lie 0.10 and 0.06 eV below that of the homoleptic **4**, consistent with the corresponding 0.09 and 0.06 V difference in the corresponding measured $E_{1/2}([Ru]^{2+/+})$ values (Table 1).

Selected unoccupied MOs of **2** are displayed in Figure 4b, showing that the LUMO of **2** is centered solely on the portion of the dppp2 ligand distal to the metal, while the LUMO+1 is localized on the portion of the same ligand proximal to the metal. The LUMO+2 and LUMO+3, also shown in Figure 4b, exhibit significant contribution from orbitals from the ancillary bpy ligands. The LUMO+1, LUMO+2, and LUMO+3 of **2** were calculated to lie 0.54, 0.63, and 0.66 eV above the LUMO, respectively. The calculated energies and corresponding electron densities of the low-lying unoccupied orbitals of **2** demonstrate that the MOs with contribution from the distal portion of the dppp2 ligand are easier to reduce than those with electron density proximal to the metal or on the ancillary bpy ligands. Similar to that of **2**, the electron densities of the LUMOs of **3** and **4** were also calculated to be localized on the distal portion of the dppp2 ligand (Figure S2). It should also be noted that for **3** the LUMO and LUMO+1 exhibit orbital contributions distal to the metal, whereas LUMO+2 and LUMO+3 possess electron density proximal to the metal. In contrast, contributions from proximal orbitals are not observed in the LUMO, LUMO+1, or LUMO+2 of **4**, only in the LUMO+3 (Figure S2). The results for **2**−**4** can be compared to those of **1** in Figure 4a, for which the energies of the lowest energy unoccupied MOs with electron density proximal to the metal center lie at similar energies and are believed to contribute to the strong MLCT transition in the absorption spectra of the complexes with maxima at 440−450 nm. However, the emission of the complexes arising from transitions associated with the LUMO is highly dependent on the energy of this orbital and shifts significantly among the complexes.

Excited State Description and Comparison to Related Complexes. Marked solvent dependence of the emission maximum and lifetime has been previously reported for related mononuclar and dinuclear Ru(II) complexes possessing ligands with extended π-systems. In such complexes, several low-lying MLCT excited states play a role in the observed photophysical properties.

As discussed above, fast internal conversion (IC) between low-lying ^3MLCT states has been reported for $[(phen)_2Ru(tpphz)Ru(phen)_2]^{4+}$, where the decay of $^3MLCT^{prox}$ and concomitant formation of $^3MLCT^{dis}$

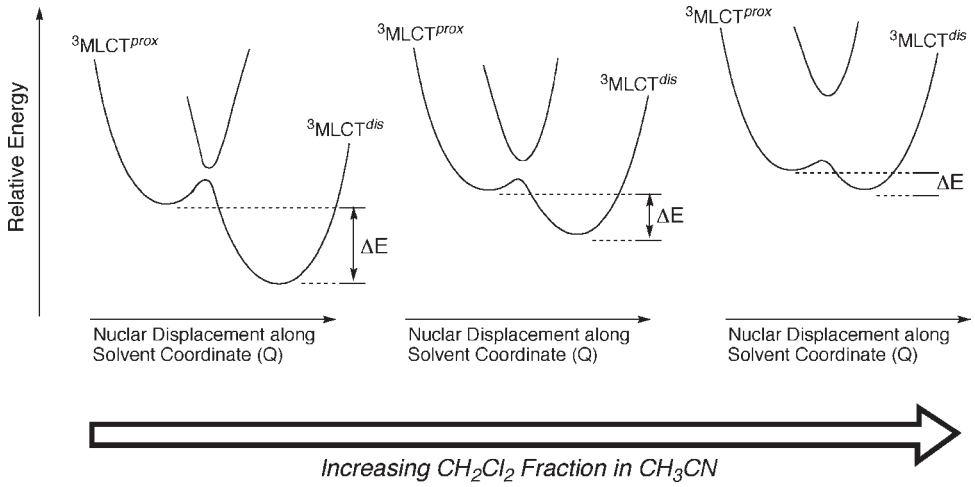

Figure 6. Schematic representation of the shift in the potential energy surfaces of the low-lying excited states along the solvent coordinate of **2**−**4** with increasing fraction of CH_2Cl_2 in CH_3CN.

take place in ~200 ps.[23] The ability to directly observe higher energy ^{3}MLCT states in Ru(II) complexes is unusual, since the IC rates are typically very fast, as is likely also the case in **2**−**4**.[23,41] Therefore, the luminescence of **2**−**4** is expected to originate from the lowest energy state, ^{3}MLCT^{dis}. However, the calculations presented here and experimental data on related molecules predict the presence of a nearby state, ^{3}MLCT^{prox}, at slightly higher energy than ^{3}MLCT^{dis}.[7b] In general, ^{3}MLCT^{prox} is expected to be highly emissive, whereas the luminescence from ^{3}MLCT^{dis} is expected to be weak if present.

The dipole moments of the ground state and the lowest energy triplet state of **1**−**4** were calculated in CH_3CN and CH_2Cl_2 treating the solvent as a continuum (Table S1). A transition dipole moment of 14.1 ± 6.1 D was reported for **1** in CH_3CN based on fits of its absorption spectrum,[42] and a dipole moment change of 8.8 ± 0.7 D for the complex was determined in alcohol at 77 K by Stark effect spectroscopy.[43] $[Ru(phen)_3]^{2+}$ was reported to exhibit a 6.7 ± 1 D dipole moment change from the ground state to the ^{1}MLCT and an estimated 11 ± 4 D difference in dipole moment between its singlet and triplet states.[44] The ground state dipole moment of **1** was calculated to be 0 D, and the dipole moment difference between the ground state and the lowest triplet state was calculated to be 9.2 D in CH_3CN and 8.8 D in CH_2Cl_2 (Table S1). The dipole moment changes calculated for **1** are in good agreement with reported experimental results.[42−44] Without ligands with an extended π-system, the dipole moment difference in **1** is nearly invariant from CH_2Cl_2 to CH_3CN (Figure 5). However, a large increase in the dipole moment difference between the ground state and the lowest triplet state of **2** is calculated with increase in solvent polarity, with a value of 15.0 D in CH_2Cl_2 and 19.4 D in CH_3CN, indicating that the lowest energy triplet state, ^{3}MLCT^{dis}, is more stabilized in CH_3CN than in CH_2Cl_2. Furthermore, as shown in Figure 5, the dipole moment difference decreases from **2** to **4** as the number of dppp2 ligands increases, implying the ^{3}MLCT^{dis} of **2** is more stabilized than those of **3** and **4**, which is supported by the emission maxima across the series of complexes.

From the dependence of the emission maximum on the solvent polarity factor, $[(\varepsilon_s - 1)/(2\varepsilon_s + 1)] - 0.5[(\varepsilon_{op} - 1)/(2\varepsilon_{op} + 1)]$, where ε_s and ε_{op} are the static and optical dielectric constants of the solvent mixture, linear fits with slopes of $(-6.5 \pm 1.6) \times 10^3$ and $(-28.7 \pm 3.9) \times 10^3$ cm^{-1} can be obtained for complexes **1** and **2**, respectively.[45] These values can be used to calculate the solvent cavity diameter (d) of a complex if its excited state dipole moment is also available according to Weller's model,[45a] resulting in $d = 4.2$ and 4.1 Å for **1** in CH_3CN and CH_2Cl_2, respectively. These values correlate well with the near invariance of the emission maximum of **1** in these solvents and are also consistent with the distance from the ruthenium to the center of the π^* orbitals on the bpy ligands (~3.7 A). Similarly, the solvent cavity diameters were also calculated for **2**, resulting in $d = 6.0$ and 5.3 Å in CH_3CN and CH_2Cl_2, respectively. The longer calculated distance in CH_3CN is consistent with the larger dipole moment of the lowest triplet state of **2** in CH_3CN compared to that in CH_2Cl_2. The distance in **2** from the ruthenium to the nitrogen atoms in the phenazine ring of the dppp2 ligand is ~6.6 Å, based on the optimized geometry (Figure S1). These results are consistent with the emission of **2** arising from ^{3}MLCT^{dis} in both solvents.

The solvent dependence of the luminescence of **2**−**4** can be explained using the simple model shown in Figure 6. In a polar solvent, such as CH_3CN, the ^{3}MLCT^{dis} state is highly stabilized because of its large dipole moment, thus it lies at a significantly lower energy than ^{3}MLCT^{prox}. From the energy gap law, it can be predicted that such stabilization results in low energy emission with short lifetime and low quantum yield. In a low polarity solvent such as CH_2Cl_2, ^{3}MLCT^{dis} is destabilized, such that it is closer in energy to ^{3}MLCT^{prox}, resulting in a longer lived emissive state with greater quantum yield. On the basis of

(41) (a) Damrauer, N. H.; Cerullo, G.; Yeh, A. T.; Boussie, T. R.; Shank, C. V.; McCusker, J. K. *Science* **1997**, *275*, 54. (b) Yeh, A. T.; Shank, C. V.; McCusker, J. K. *Science* **2000**, *289*, 935.
(42) Kober, E. M.; Sullivan, B. P.; Meyer, T. J. *Inorg. Chem.* **1984**, *23*, 2098.
(43) Oh, D. H.; Boxer, S. G. *J. Am. Chem. Soc.* **1989**, *111*, 1130.
(44) Karki, L.; Hupp, J. T. *Inorg. Chem.* **1997**, *36*, 3318.
(45) (a) Beens, H.; Knibbe, H.; Weller, A. *J. Chem. Phys.* **1967**, *47*, 1183. (b) Wasielewski, M. R.; Minsek, D. W.; Niemczyk, M. P.; Svec, W. A.; Yang, N. C. *J. Am. Chem. Soc.* **1990**, *112*, 2823.

the photophysical data of **2**−**4**, it is predicted that the luminescence of each complex arises from the $^3MLCT^{dis}$ state and that the interconversion between $^3MLCT^{prox}$ and $^3MLCT^{dis}$ must be at least an order of magnitude greater than the decay from $^3MCLT^{dis}$.[46,47] This prediction is indeed confirmed by the results of femtosecond transient absorption spectroscopy.[48] As recently reported by our group, the ultrafast dynamics of the interconversion between the two ^3MLCT states in **2** is highly dependent on solvent polarity, showing a rise time of the $^3MCLT^{dis}$ state of 67 and 26 ps in CH_2Cl_2 and CH_3CN, respectively, from the initially populated $^3MLCT^{prox}$ state.[48]

Conclusions

The synthesis, characterization, and photophysical properties of a series of ruthenium complexes that possess the dppp2 ligand are presented. Different from the relatively strong luminescence and relatively insensitive emission maximum of $[Ru(bpy)_2(dppz)]^{2+}$ and **1** in organic solvents, the photophysical properties of **2**−**4** exhibit a strong dependence on solvent polarity. The luminescence quantum yield of **2** is 19-fold greater in CH_2Cl_2 than in CH_3CN, and a large red shift of the emission maximum from 653 nm in CH_2Cl_2 to 752 nm in CH_3CN is also observed. Electrochemistry and theoretical calculations suggest that such a strong dependence on solvent polarity results from the greater stabilization of the excited state localized on the distal portion of the dppp2 ligand, $^3MLCT^{dis}$, in the polar solvent compared to that localized on the proximal part of dppp2, $^3MLCT^{prox}$. Transient absorption experiments show that the identity of the excited state is the same in CH_3CN and CH_2Cl_2. The smooth variation of the emission spectra of **2** in CH_3CN/CH_2Cl_2 mixtures demonstrates that the energy of its lowest excited state can be gradually raised through the addition of CH_2Cl_2 to CH_3CN. In contrast to $[Ru(bpy)_2(dppz)]^{2+}$, the lowest energy excited state in the dppp2-containing complexes is assigned as arising from a triplet MLCT state where the charge is localized on the portion of the dppp2 ligand distal to the metal, $^3MLCT^{dis}$. The larger charge separation distance in $^3MLCT^{dis}$ compared to $^3MLCT^{prox}$ makes the former more sensitive than the latter to changes in solvent polarity. Overall, the strong solvent dependence of the luminescence of **2**−**4**, including the large shift of the emission maximum, makes these complexes potential candidates for various sensing applications.

Acknowledgment. C.T. thanks the National Science Foundation (CHE-0911354) and the Ohio Supercomputer Center for their generous support.

Supporting Information Available: Calculated dipole moments and distances among atoms of interest in **2** and selected unoccupied molecular orbitals of **3** and **4**. These materials are available free of charge via the Internet at http://pubs.acs.org.

(46) Olson, E. J. C.; Hu, D.; Hormann, A.; Jonkman, A. M.; Arkin, M. R.; Stemp, E. D. A.; Barton, J. K.; Barbara, P. F. *J. Am. Chem. Soc.* **1997**, *119*, 11458.
(47) Onfelt, B.; Lincoln, P.; Nordén, B.; Baskin, J. S.; Zewail, A. H. *Proc. Natl. Acad. Sci.* **2000**, *97*, 5708.
(48) Sun, Y.; Liu, Y.; Turro, C. *J. Am. Chem. Soc.* **2010**, *132*, 5594.